Soft Matter

Accepted Manuscript

ROYAL SOCIETY OF CHEMISTRY

www.rsc.org/softmatter

Magnetic cylindrical colloids at liquid interfaces exhibit non-volatile switching of their orientation in an external field

Bethany J. Newton, D. Martin A. Buzza*

Theory of Condensed Matter Group, Department of Physics and Mathematics, University of Hull, Hull, HU6 7RX, UK

May 12, 2016

Abstract

We study the orientation of magnetic cylindrical particles adsorbed at a liquid interface in an external field using analytical theory and high resolution finite element simulations. Cylindrical particles are interesting since they possess multiple locally stable orientations at the liquid interface so that the orientational transitions induced by an external field will not disappear when the external field is removed, i.e., the switching effect is *non-volatile*. We show that, in the absence of an external field, as we reduce the aspect ratio α of the cylinders below a critical value ($\alpha_c \approx 2$) the particles undergo spontaneous symmetry breaking from a stable side-on state to one of two equivalent stable tilted states, similar to the spontaneous magnetisation of a ferromagnet going through the Curie point. By tuning both the aspect ratio and contact angle of the cylinders, we show that it is possible to engineer particles that have one, two, three or four locally stable orientations. We also find that the magnetic responses of cylinders with one or two stable states are similar to that of paramagnets and ferromagnets respectively, while the magnetic response of systems with three or four stable states are even more complex and have no analogs in simple magnetic systems. Magnetic cylinders at liquid interfaces therefore provide a facile method for creating switchable functional monolayers where we can use an external field to induce multiple non-volatile changes in particle orientation and self-assembled structure.

1 Introduction

Particles adsorbed at fluid interfaces are of broad interest to a wide range of soft matter systems, from particle stabilised emulsions and foams,[1,2] to membrane and interfacial proteins,[3] to functional surfaces for nanotechnology.[4,5] Most of the research in this area has focused on spherical or nearly spherical particles. However, with advances in the

*Author to whom correspondence should be addressed. Email: d.m.buzza@hull.ac.uk

synthesis of colloidal particles, particles with other shapes have received increasing attention over the last decade. These shapes include ellipsoids,[6–9] cylinders,[10,11] cubes[12] and more exotic shapes.[13] The behaviour of such anisotropic particles at fluid interfaces is even richer than that of spherical particles for two reasons. Firstly, anisotropic particles can adopt multiple locally stable orientations at the liquid interface.[10,12–17] Secondly, for non-neutrally wetting particles (i.e., contact angle $\theta_w \neq 90°$), the constant contact angle requirement at the three phase contact line leads to significant deformations of the liquid meniscus around the anisotropic particles and hence strong capillary interactions between particles.[6–9,11,18–20] Both the orientation of individual particles and the capillary interaction between particles are strongly dependent on the shape of the anisotropic particle. For example, for ellipsoidal particles, the equilibrium orientation is always 'side-on' (i.e., particle long axis parallel to liquid interface),[8,16] while for cylindrical particles, the equilibrium orientation can be 'side-on' or 'end-on' (i.e., particle long axis perpendicular to liquid interface).[10] In addition, while the far-field capillary interactions between both ellipsoidal and cylindrical particles are quadrupolar,[6–9,11,18,19] the near-field capillary interactions are strongly shape dependent, causing ellipsoidal particles to prefer to assemble side-to-side (identical ellipsoids) or at an angle (non-identical ellipsoids) and cylindrical particles to prefer to assemble tip-to-tip.[18,19,21]

By imposing external fields on particles at liquid interfaces such as electric,[22] magnetic[5,23,24] or interfacial curvature,[25,26] it is possible to gain further control over the assembly of particles at liquid interfaces, opening up exciting opportunities for creating switchable functional surfaces. In this paper, we focus on controlling the orientation of anisotropic particles using magnetic fields. Recent studies have shown that for magnetic ellipsoidal particles adsorbed at a liquid interface, when an external field is applied perpendicular to the liquid interface, it is possible to stabilise tilted configurations of the ellipsoidal particles, and above a critical field strength, the ellipsoidal particles undergo an irreversible orientational transition to the end-on state.[14–16] For neutrally wetting ellipsoidal particles ($\theta_w = 90°$) where quadrupolar deformations of the meniscus are absent, Davies et al.[5,24] have also shown in their seminal work that the tilted orientation of the particles leads to dipolar capillary interactions between particles that can be used to create a switchable system where the self-assembled structure can be controlled using an external field.[5] However, one drawback of ellipsoidal particles is that because the

side-on state is the only stable orientation in the absence of an external field, as soon as the external field is removed, the ellipsoidal particles revert to the side-on state and all memory of particle orientation and self-assembled structure is lost, i.e., the switching effect is *volatile*.

In order to overcome this problem, in this paper we study the orientation of magnetic *cylindrical* particles adsorbed at a liquid interface in an external field. The advantage of cylindrical particles is that, because of the flat end of the cylinder, cylinders can possess multiple locally stable orientations in the absence of an external field, including side-on and end-on states as shown by Lewandowski et al.[10] This means that for cylindrical particles, orientational transitions induced by an external field will not necessarily disappear when the external field is removed, i.e., the switching effect can be *non-volatile*.

We will analyse this problem theoretically using both a simplified thermodynamic model which assumes the liquid meniscus around the particle is flat and a high resolution finite element method (Surface Evolver[27]) which accurately captures the meniscus deformation around the particle. In contrast to previous studies which only considered end-on and side-on states,[10] we also consider all intermediate particle orientations and find that the behaviour for cylindrical particles is even richer than hitherto anticipated. For example, we find that even in the absence of an external field, cylindrical particles can possess not only stable side-on and end-on states, but also stable *tilted* states, depending on the aspect ratio $\alpha = L/2r$ of the particle (where L and r are the length and radius of the cylinder respectively). Our calculations show that tilted configurations with perceptible tilt angles occur for aspect ratios in the range $0.5 \lesssim \alpha \lesssim 2$; this would explain why these tilted states have not been observed previously in experimental studies, as only smaller and larger α were investigated in detail.[10] Such tilted states have been predicted for exotic anisotropic Janus particles,[3,28–30] but to our knowledge this is the first time that their existence has been discussed explicitly for anisotropic colloids with homogeneous surface chemistry. In addition, by tuning both the aspect ratio α and contact angle θ_w, we show that it is possible to engineer cylindrical particles to have two, three or even four locally stable orientations which can be accessed by varying the external field. Such a system allows us to create switchable functional colloidal monolayers where we can induce multiple *non-volatile* changes in optical, magnetic and mechanical properties using an external field.

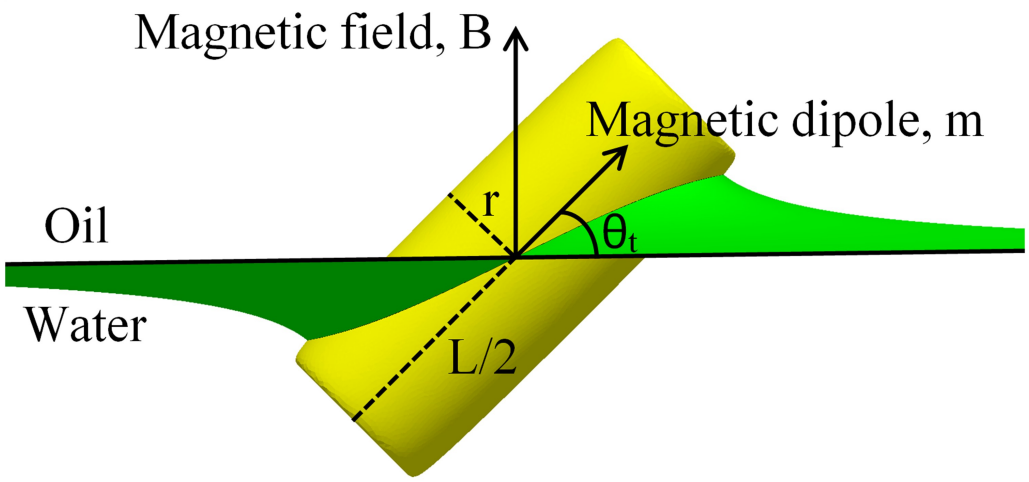

Figure 1: Configuration of a cylindrical particle adsorbed at an oil/water interface in the presence of an external field B applied perpendicular to the interface. The variables characterising the geometry of the tilted particle are discussed in the main text. The image is generated from Surface Evolver simulations of a cylinder with contact angle $\theta_w = 90°$, aspect ratio $\alpha = 2.5$, tilt angle $\theta_t = 45°$ and sharpness parameter $\eta = 20$ and the deformation of the liquid meniscus has been taken into account.

The rest of this paper is organised as follows. In section 2, we discuss the thermodynamics of the system and provide details of the flat interface model and the Surface Evolver method. In section 3, we present results for the orientational behaviour of magnetic cylinders at liquid interfaces and discuss their relevance for creating switchable functional surfaces and the feasibility of realising these results experimentally. Finally in section 4 we summarise our key conclusions.

2 Theoretical Methods

2.1 Thermodynamic Model

We consider a cylindrical particle with length L and radius r adsorbed at an interface between two immiscible liquids (Figure 1). For convenience, we will refer to the top liquid as 'oil' and the bottom liquid as 'water' in what follows. The cylinder has an embedded magnetic dipole m along the long axis of the particle and the particle is tilted such that the magnetic dipole is at an angle θ_t with respect to the unperturbed interface. The aspect ratio of the cylindrical particle is defined as $\alpha = L/2r$, and the magnetic dipole interacts with an external magnetic field B applied perpendicular to the interface.

The total free energy of the three phase system is given by

$$F_{int} = \gamma_{ow}A_{ow} + \gamma_{po}A_{po} + \gamma_{pw}A_{pw} - mB\sin\theta_t \tag{1}$$

where γ_{ow},γ_{po},γ_{pw} are the interfacial tensions and A_{ow},A_{po},A_{pw} are the areas of the oil/water, particle/oil and particle/water interfaces respectively. The free energy in eq.(1) can be simplified to the dimensionless form[16]

$$\bar{F}_{int} \equiv \frac{F_{int}}{\gamma_{ow}A_p} = \overline{A}_{ow} + \cos\theta_w\overline{A}_{po} - \overline{B}\sin\theta_t \tag{2}$$

where $\overline{A}_{ow} = A_{ow}/A_p$, $\overline{A}_{po} = A_{po}/A_p$ are the dimensionless oil/water and particle/oil areas respectively, A_p is the surface area of the cylindrical particle, $\overline{B} = mB/\gamma_{ow}A_p$ is the dimensionless magnetic field strength and θ_w is the contact angle of the oil/water interface at the particle surface. Obviously we can readily convert the dimensionless free energy to the free energy in units of k_BT by multiplying the dimensionless free energy with the factor $\gamma_{ow}A_p/k_BT$ for the relevant particle.

Minimizing $\overline{F}_{int}$ with respect to θ_t for a given value of $\overline{B}$ allows us to determine the equilibrium tilt angle of the particle for a given magnetic field strength. Note that minimizing $\overline{F}_{int}$ is equivalent to solving the equation

$$\frac{1}{\cos\theta_t}\frac{\partial\overline{F}_{st}}{\partial\theta_t} = \overline{B} \tag{3}$$

where

$$\overline{F}_{st} = \overline{A}_{ow} + \cos\theta_w\overline{A}_{po} \tag{4}$$

is the free energy contribution from the interfacial tension terms. Thus by calculating the interfacial energy $\overline{F}_{st}$ and $\frac{\partial\overline{F}_{st}}{\partial\theta_t}$ as a function of θ_t, we can determine the equilibrium tilt angle for a given $\overline{B}$ via eq.(3).[16] This is the method we use to calculate the magnetic response of the cylindrical systems in this paper, including equilibrium tilt angles, critical fields and critical angles (see Supplementary Information).

The interfacial free energy $\overline{F}_{st}$ is calculated in two ways in this paper. In the first approach, following Bresme and Faraudo, we assume that the oil/water meniscus around the adsorbed cylinder is flat.[14] This simplifying assumption allows us to calculate $\overline{A}_{ow}$ analytically and we will use this method to study the case of neutrally wetting cylinders ($\theta_w = 90°$) where the $\overline{A}_{po}$ term in eq.(4) can be neglected. In the second approach, we calculate both $\overline{A}_{po}$ and $\overline{A}_{ow}$ numerically using the finite element method Surface

Evolver.[27] This approach allows us to accurately model the deformation of the oil/water meniscus around the particle and we will use this method to analyse both neutrally wetting and non-neutrally wetting cylinders ($\theta_w \neq 90°$).

2.2 Flat Interface Model

In this subsection, we calculate the interfacial free energy (eq.(4)) for a cylinder of length L, radius r, assuming the liquid interface remains flat in the presence of the adsorbed cylinder. To simplify our calculation, we consider the neutrally wetting case $\theta_w = 90°$ where the cylinder centre is located at the interface plane and the particle rotates about its centre and we can neglect the $\overline{A}_{po}$ term in eq.(4). In the flat interface model, the area of the oil/water interface in the presence of the adsorbed particle is simply given by

$$A_{ow} = A_0 - A_{st} \tag{5}$$

where A_0 is an (uninteresting) constant representing the total area of the oil/water interface in the absence of the adsorbed particle and A_{st} is the intersection area between the cylinder and the flat interface. Our task is therefore to calculate A_{st} as a function of tilt angle θ_t. Without loss of generality, we assume that the particle centre is at the origin, the interfacial normal is in the z direction, the particle rotates about the x-axis and the long axis of the cylinder is in the y direction when it is in the side-on state (Figure 2).

We first define the critical tilt angle β as the angle where the liquid interface just intersects the flat ends of the cylinder (Figure 2(c),(d)). From simple geometry, $\tan\beta = 2r/L$. For $\theta_t > \beta$, the liquid interface does not intersect the flat ends of the cylinder (Figure 2(a)) and the intersection between the interface and the cylinder is therefore an ellipse with semi-minor axis $a = r$ and semi-major axis $b = r/\sin\theta_t$ (Figure 2(b)). In this case, the intersection area is given by

$$A_{st} = \pi ab = \frac{\pi r^2}{\sin\theta_t}, \quad (\theta_t > \beta) \tag{6}$$

For $\theta_t \leq \beta$, the liquid interface intersects the ends of the cylinder (Figure 2(e)) and the intersection between the interface and the cylinder is therefore an ellipse with semi-minor axis $a = r$ and semi-major axis $b = r/\sin\theta_t$ which is truncated at $y = \pm\tilde{b}$ (Figure 2(f)), where $\tilde{b} = L/(2\cos\theta_t)$. Noting that the equation for the ellipse is $(x/r)^2 + (y/b)^2 = 1$,

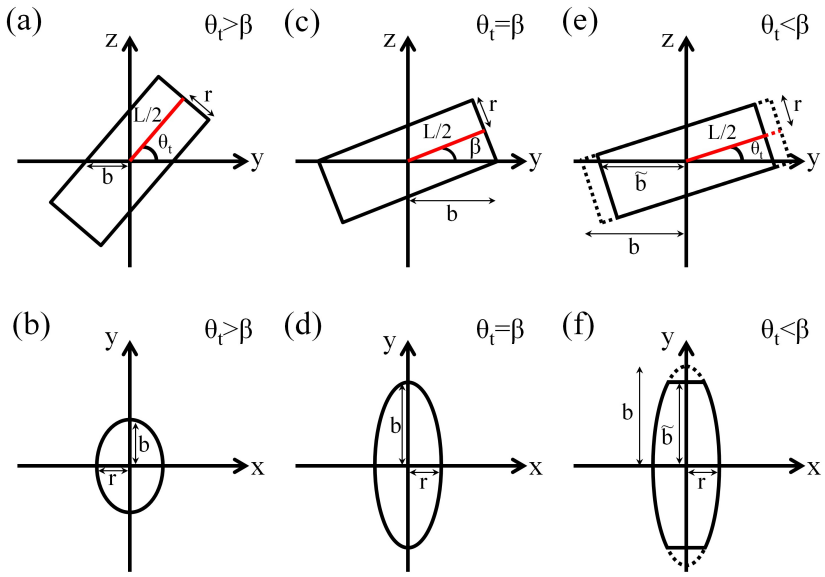

Figure 2: Configuration of a cylinder with $\theta_w = 90°$ at an oil/water interface for different tilt angles, assuming the oil/water interface remains flat. Here $\beta = \tan^{-1} 2r/L$ is the critical tilt angle where the liquid interface just intersects the flat ends of the cylinder. (a), (c), (e) represent the side view of the cylinder while (b), (d), (f) represent the intersection between the flat interface and the cylinder.

the intersection area in this case is given by

$$\begin{aligned} A_{st} &= 4\int_0^{\tilde{b}} x(y)dy = 4a\int_0^{\tilde{b}} \sqrt{1-\frac{y^2}{b^2}}dy \\ &= \frac{Lr}{\cos\theta_t}\left[\sqrt{1-f(\theta_t)^2} + \frac{\sin^{-1} f(\theta_t)}{f(\theta_t)}\right], \quad (\theta_t \le \beta) \end{aligned} \tag{7}$$

where $f(\theta_t) = \alpha \tan\theta_t$.

2.3 Surface Evolver Method

In this subsection, we provide details for the finite element package Surface Evolver[27] that we use to calculate the interfacial free energy and equilibrium meniscus shape around a cylindrical particle. One problem with using finite element methods to analyse the orientational behaviour of cylinders is that the method becomes numerically unstable when the three phase contact line crosses the sharp edge of the cylinder. To overcome this problem, we approximate the cylinder using the super-ellipsoid equation[18]

$$\left(\frac{z^2}{r^2} + \frac{x^2}{r^2}\right)^{\eta} + \left(\frac{2y}{L}\right)^2 = 1 \tag{8}$$

where η is the sharpness parameter, with $\eta = 1$ and $\eta = \infty$ corresponding to an ellipsoid and a cylinder with infinitely sharp edges respectively. In our calculations, we use $\eta = 20$

which corresponds to a cylinder with slightly rounded edges (see fig.1); we find that this value of η represents a good compromise between numerical accuracy and stability (see Supplementary Information). From an experimental point of view, studying cylinders with slightly rounded edges is also interesting in its own right since cylinders with infinitely sharp edges are an idealised limiting case and real cylinders will inevitably have slightly rounded edges.

In our simulations, the cylinder is gradually tilted from 0° to 90° in 1° increments; only tilt angles $0° \leq \theta_t \leq 90°$ need to be explicitly calculated since, in the absence of an external field, the orientational free energy is symmetric about $\theta_t = 0°$. The oil-water and particle-oil interfaces are divided into a mesh of small triangles which are displaced to minimise the interfacial energy subject to appropriate constraints. Specifically, we apply the super-ellipsoid equation (eq.(8)) on the vertices representing the particle and the contact line where the particle meets the oil-water interface. For computational convenience and without loss of generality, the centre of the particle is fixed at the origin of coordinate system used and the interface is free to move vertically to satisfy the contact angle.[16] Also, the homogeneous Neumann boundary condition is used at the outer boundary of the simulation domain to ensure a flat interface far from the particle.[11] We calculate the area of the interface by adding up the individual facets of the triangulated mesh. We compared results for $\eta = 1$ (i.e., ellipsoidal particle) with previously published results[16] to confirm that the method gave the same results. In order to achieve good numerical accuracy we used a mesh that has a higher level of refinement close to the particle. In the last stages of the evolution we change the model type from linear to quadratic which adds vertices at the midpoints of each edge followed by further minimisation which allows us to evaluate the areas with high accuracy. For example, for particles with an aspect ratio $\alpha = 2.5$, contact angle $\theta_w = 90°$ and tilt angle $\theta_t = 45°$, we used 140000 triangles to represent the surface and 848 vertices to represent the contact line; the specific number of triangles and vertices used was varied depending on the values of α, θ_w and θ_t. We use a square simulation box which has length $12 \times L$ for $\alpha > 1$, or length $12 \times r$ for $\alpha < 1$, and we work in units of length where $r = 1$. In order to confirm that finite size constraints are negligible, for selected simulations, the simulation cell size was increased by 50% and yielded essentially the same results for the critical tilt angles (within 0.5%) and critical field strength (within 0.3%).

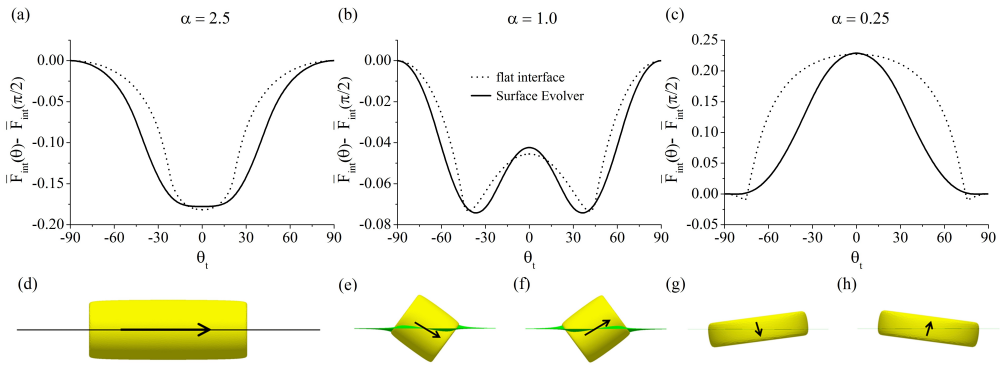

Figure 3: (a)-(c) Dimensionless free energy (relative to the end-on configuration) as a function of tilt angle for cylindrical particles in the absence of an external field with contact angle $\theta_w = 90°$ and different aspect ratios α calculated from flat interface theory (dashed line) and Surface Evolver simulations with $\eta = 20$ (solid line); (d)-(h) Equilibrium configurations of the particle for the different values of α obtained from Surface Evolver simulations. The specific tilt angles are (d) 0°; (e) −36.4°; (f) +36.4°; (g) −82.6°; (h) +82.6°.

3 Results and Discussion

3.1 Neutrally Wetting Cylinders ($\theta_w = 90°$)

We first study the equilibrium orientation of neutrally wetting cylinders adsorbed at the interface in the absence of an external field. In contrast to previous studies which only considered the side-on and end-on states,[10] we also consider all intermediate particle orientations. In Figure 3(a)-(c), we plot the dimensionless free energy vs. tilt angle θ_t for $\theta_w = 90°$ for three different aspect ratios $\alpha = 2.5, 1.0, 0.25$ respectively. The dashed lines are the predictions of the flat interface model while the solid lines are the predictions of Surface Evolver which takes into account the deformation of the meniscus. Figure 3(d)-(h) are the equilibrium orientations for the different values of α predicted by Surface Evolver. Focussing first of all on the predictions of the flat interface theory, we see that for large α (e.g., $\alpha = 2.5$, Figure 3(a)), the side-on state ($\theta_t = 0°$) is the equilibrium state, i.e., the global minima of the free energy. In addition, as we decrease α, the side-on state becomes less stable relative to the end-on state ($\theta_t = 90°$) such that for small α (e.g., $\alpha = 0.25$, Figure 3(c)) the end-on state is more stable than the side-on state. These results are in good agreement with previous studies.[10]

However our fuller analysis reveals the surprising result that for small aspect ratios α (below a critical value $\alpha_c \approx 2$), the equilibrium state is not the end-on state anticipated in previous studies,[10] but a tilted configuration (Figure 3(b),(c)). Furthermore, the equi-

librium tilt angle increases with decreasing α such that for very small α the equilibrium tilt angle is very close to $\theta_t = 90°$. All the qualitative features predicted by the flat interface theory are corroborated by the Surface Evolver results (Figure 3(a)-(c) solid lines), with the quantitative differences between the two theories being due to the fact that Surface Evolver explicitly accounts for interfacial deformation and uses slightly rounded edges. Note that both flat interface theory and the Surface Evolver calculations predict that tilted configurations with perceptible tilt angles only occur for aspect ratios in the range $0.5 \lesssim \alpha \lesssim 2$; this would explain why these tilted states have not been observed previously in experimental studies of neutrally wetting cylinders,[10] as only smaller and larger α were investigated in detail in these studies.

We note the striking resemblance between the free energy curves in Figure 3 and those for spontaneous symmetry breaking in ferromagnets under zero field conditions.[31] Making this analogy between the two systems, the side-on state (Figure 3(a)) corresponds to the paramagnetic state, the tilted state (Figure 3(b),(c)) corresponds to the ferromagnetic state and the aspect ratio α plays the role of temperature. We emphasize that this analogy is purely mathematical since we are performing single particle simulations throughout this paper, while in real ferromagnets, the spontaneous magnetisation is due to many-body interactions between neighbouring magnetic dipoles. Notwithstanding this important *physical* difference between the two systems, our mathematical analogy is nevertheless useful in helping us anticipate the magnetic response of single cylinders at liquid interfaces. Specifically, it suggests that the response of cylinders with $\alpha > \alpha_c$ and $\alpha < \alpha_c$ to an external magnetic field should be similar to that of paramagnets and ferromagnets respectively, an expectation which is confirmed later on (see Figure 5).

By performing a series expansion (i.e., Landau expansion) of $\overline{F}_{st}$ in θ_t about $\theta_t = 0°$ for the flat interface theory (i.e., using eqs.(5),(7) in eq.(4)) to quadratic order, we find

$$\overline{F}_{st} = \text{const} + \frac{\alpha^2}{3\pi(1+2\alpha}(\alpha^2 - 3)\theta_t^2. \tag{9}$$

Noting that the critical aspect ratio is the aspect ratio where the quadratic coefficient in the Landau expansion vanishes, eq.(9) predicts that $\alpha_c = \sqrt{3}$. This value for α_c from the flat interface theory is slightly lower that the value deduced from our Surface Evolver calculations for neutrally wetting cylinders, i.e., $\alpha_c \approx 2.3$ (see Figure 11 and Table 2 in Supplementary Information).

An interesting question concerns the symmetry of meniscus deformations around par-

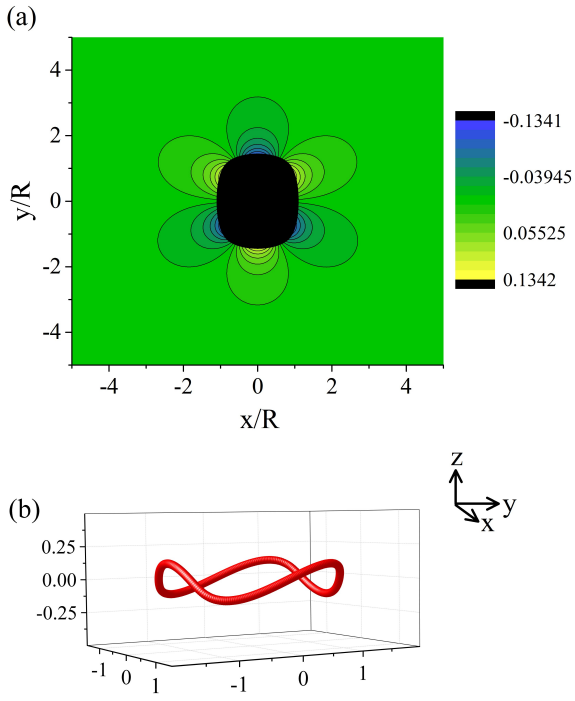

Figure 4: Surface Evolver results for (a) the meniscus deformation (contour plot) and (b) contact line around a cylindrical particle in the equilibrium tilted configuration with $\theta_w = 90°$, $\alpha = 1$, $\eta = 20$ ($\theta_t = 36.4°$). Note the clear hexapolar symmetry of the deformation.

ticles in the equilibrium tilted state for $\alpha < \alpha_c$. Naively, one might expect the leading order deformation to be dipolar. However, dipolar deformations are forbidden as there is no external torque acting on the particle at equilibrium.[19,32] In Figure 4(a),(b), we plot the Surface Evolver results for the deformation field and contact line respectively around a cylindrical particle in the equilibrium tilted state with $\theta_w = 90°$ and $\alpha = 1$. We see that the deformation is in fact neither dipolar nor quadrupolar but *hexapolar*. Under zero bond number conditions (i.e., where gravity is negligible), the leading order distortion that is allowed is quadrupolar,[19,32] and indeed for simple anisotropic shapes like ellipsoids, the leading order distortion is always quadrupolar.[6–8] However, for more complex particles shapes, it is possible to have leading order deformations which are of a higher order multipole. For example, the leading order distortion for cuboidal particles has recently been shown to be octupolar.[17] The theoretical framework for the interaction between capillary multipoles of arbitrary order has been worked out by Danov et al.[33]

Next, we consider the response of neutrally wetting cylindrical particles to an external field applied perpendicular to the liquid interface. In Figure 5(a), we plot the Surface

Evolver results for the free energy as a function of tilt angle for cylinders with $\alpha = 2.5 > \alpha_c$. At zero field, the equilibrium state is the side-on state (black curve), but as we increase the field strength, the equilibrium state shifts to a tilted state with finite tilt angle (e.g., blue curve), with the equilibrium tilt angle increasing with increasing field strength. As the field strength is further increased above a critical field $\overline{B}_{c1}$, the free energy curve develops a second minima at $\theta_t = 90°$ corresponding to the end-on state, and at a field strength of $\overline{B} = \overline{B}_0 = 0.288$, the free energy of the tilted state becomes equal to that of the end-on state (green curve, see inset). At this point, the particle in principle undergoes a first order phase transition from the tilted state to the end-on state. The filled circles on the green curve with tilt angles $\theta_0 = 33.8°$ and $90°$ are therefore binodal points of the system. However, for micron sized particles (which is the focus of this paper), the very large energy barrier between the two local minima means that in practice there is significant hysteresis in the orientational transition.[16] Specifically, for increasing magnetic fields, the particle only undergoes an irreversible transition from the tilted state to the end-on state when $\overline{B} = \overline{B}_{c2}$, where the local minima for the tilted state disappears (red curve, see inset), while for decreasing field strengths, the particle only undergoes an irreversible transition from the end-on state to the tilted state when $\overline{B} = \overline{B}_{c1}$, where the local minima for the end-on state disappears (blue curve). The open circle on the red curve with tilt angle $\theta_{c2} = 43.1°$ and the end on state ($\theta_t = 90°$) on the blue curve are therefore spinodal points of the system. Analogous behaviour to everything discussed above also occurs for $\overline{B} < 0$.

The magnetic response the long cylinder ($\alpha > \alpha_c$) is summarised in Figure 5(b) where we plot the Surface Evolver results for the locally stable tilt angle ($\sin\theta_t$) as a function of the external field ($\overline{B}$) (see Supplementary Information for details of how the magnetic response was calculated). We note that, as anticipated earlier for $\alpha > \alpha_c$, the response of the cylinder is paramagnetic-like at low fields ($|\overline{B}| < \overline{B}_{c1}$), with the equilibrium tilt angle θ_t (or $\sin\theta_t$) playing the role of magnetisation in magnetic systems.[34] Specifically as we increase the magnetic field from negative to positive values, the tilt angle increases *continuously* from negative to positive. On the other hand, the response of the system exhibits significant hysteresis at higher fields ($|\overline{B}_{c1}| \leq |\overline{B}| \leq |\overline{B}_{c2}|$) as discussed earlier.

From the point of view of creating switchable materials, the key feature of Figure 5(b) is the fact that any particle orientations induced by an external field will disappear

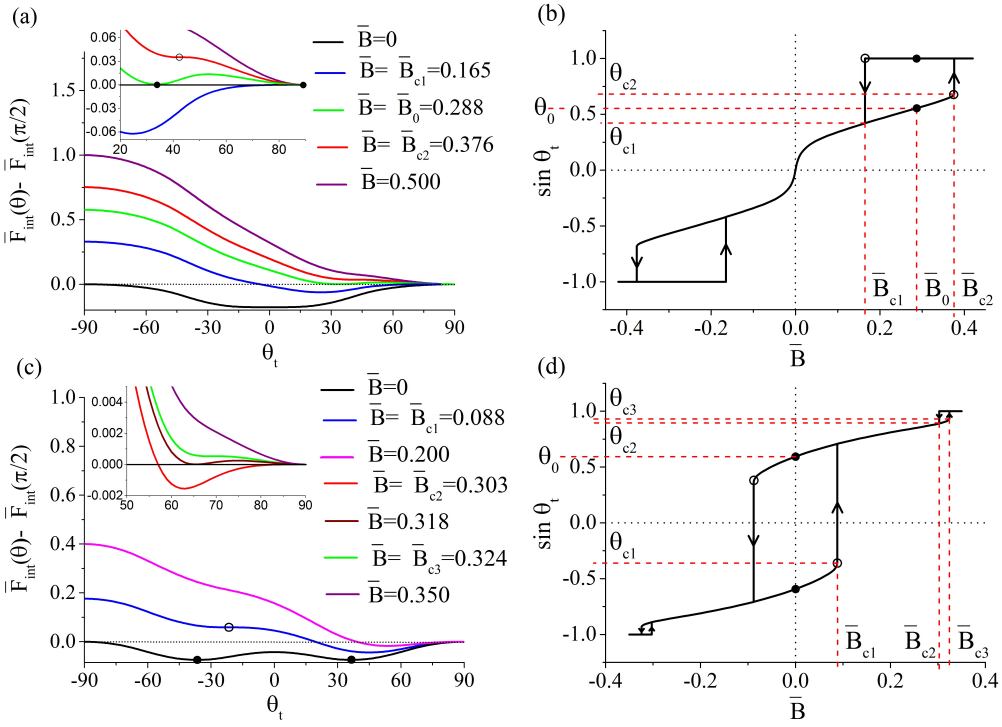

Figure 5: Surface Evolver results for the magnetic response of cylinders with $\theta_w = 90°$, $\eta = 20$. (a),(c) Dimensionless free energy as a function of tilt angle for different field strengths for: (a) $\alpha = 2.5$; (c) $\alpha = 1.0$. The insets in (a) and (c) zoom in on the large tilt angle region of the free energy curves where there is a first order orientational transition between the tilted and end-on states at large fields. (b), (d) Locally stable tilt angle as a function of field strength for: (b) $\alpha = 2.5$; (d) $\alpha = 1.0$. In (b), (d), the vertical lines represent irreversible orientational transitions, with the direction of the transition as indicated by the arrows. For all the other solid lines in (b), (d), it is possible to change the tilt angle along the line in either direction by changing the external field. In (a)-(d), the filled and open circles represent binodal and spinodal points of the orientational transitions respectively. Note that in (a), there is a spinodal point at the end-on state ($\theta_t = 90°$) on the blue curve. See main text for details.

when the external field is removed ($\theta_t = 0$ for $\overline{B} = 0$), i.e., the switching effect is *volatile*. The magnetic response of neutrally wetting long cylinders is thus qualitatively the same as that of ellipsoidal particles.[14–16]

In Figure 5(c), we plot the Surface Evolver results for the free energy as a function of tilt angle for cylinders with $\alpha = 1.0 < \alpha_c$. As discussed earlier, at zero field the cylinder can adopt either one of two equivalent tilted states (filled circles on black curve). For definiteness, let us assume that the particle is initially in the tilted state with negative tilt angle. As we increase the field strength, the degeneracy between the two tilted states is broken and the negative tilted state is no longer the global minimum. In principle therefore, the particle should undergo a first order phase transition to the positive tilted state. The filled circles in the zero-field free energy curve which have tilt angles of $\pm\theta_0$ are therefore *binodal* points of the system. However, the very large energy barrier between the local minima for micron sized particles means that in practice the orientational transition does not occur until the field strength is equal to $\overline{B}_{c1}$ where the local minima for the negative tilted state merges with the energy barrier and the local minima disappears (open circle on blue curve). The open circle on the blue curve which has a tilt angle of $-\theta_{c1}$ are therefore *spinodal* points of the system for positive external field. Similarly, if the particle is in the positive tilted state, upon decreasing the external field, the orientational transition to the negative tilted state does not occur until the field strength is equal to $-\overline{B}_{c1}$. To complete the picture, as we increase the field strength above $\overline{B}_{c3}$ (or decrease the field strength below $-\overline{B}_{c3}$), there is a further (small) first order orientational transition in the large field regime (see inset to Figure 5(c)) which leads to a small degree of hysteresis in the magnetic response between $\overline{B}_{c2} \leq |\overline{B}| \leq \overline{B}_{c3}$ (Figure 5(d)).

The magnetic response the short cylinder ($\alpha < \alpha_c$) is summarised in Figure 5(d) where we plot the Surface Evolver results for the locally stable tilt angle ($\sin\theta_t$) as a function of the external field ($\overline{B}$). The most striking feature of Figure 5(d) is the fact that the response of short cylinders at low fields ($|\overline{B}| < \overline{B}_{c3}$) is ferromagnetic-like rather than paramagnetic-like. Specifically, assuming the cylinder is initially in the negative tilted state, as we increase the magnetic field from negative to positive, thermodynamically the tilt angle undergoes a reversible, discontinuous transition from $-\theta_0$ to $+\theta_0$ at $\overline{B} = 0$ (i.e., bottom filled circle to top filled circle in Figure 5(d)). However, as discussed earlier, in practice the tilt angle undergoes an irreversible transition to the positive tilted state only

when the magnetic field exceeds $\overline{B}_{c1}$ (i.e., bottom open circle in Figure 5(d)). Analogous behaviour is also observed when we decrease the magnetic field starting from the positive tilted state.

Applying the terminology for ferromagnetic systems to Figure 5(d), the tilt angles at the binodal points, i.e., θ_0 (filled circles in Figure 5(d)), correspond to the 'remnance' of the cylinder while the magnetic field at the spinodal points, i.e., $\overline{B}_{c1}$ (open circles in Figure 5(d)), corresponds to the 'coercivity' of the system.[34] From the point of view of creating switchable materials, the key feature of Figure 5(d) is the fact that the system possesses two locally stable orientations (corresponding to the filled circles) which do not disappear when the the external field is removed and which can be accessed by varying the external field, i.e., the switching effect is *non-volatile*. This means that neutrally wetting short cylinders ($\alpha < \alpha_c$) can be used to create switchable functional surfaces with non-volatile switching.

In Figure 6, we study the magnetic response of neutrally wetting cylinders to low external fields over a more comprehensive range of α values, both above and below α_c. Specifically, we plot the Surface Evolver results for the stationary tilt angles (i.e., tilt angles corresponding to minima or maxima of the free energy curves) as a function of the external field $\overline{B}$ for different values of α, with the solid (dashed) lines corresponding to locally stable (unstable) tilt angles. The filled and unfilled circles in Figure 6 correspond to the binodal and spinodal points respectively when $\alpha < \alpha_c$. Note that the solid curves between the binodal and spinodal points are metastable while the rest of the solid curves are stable. Details of how the magnetic response for different α was calculated, including the tilt angles and magnetic fields at the binodal and spinodal points, are provided in Supplementary Information.

The magnetic response curves in Figure 6 clearly resemble the magnetisation curves for a ferromagnet as it goes through the Curie temperature. Specifically, for $\alpha > \alpha_c$, the magnetic response is paramagnetic-like (c.f. Figure 5(b)) while for $\alpha < \alpha_c$, the response becomes ferromagnetic-like (c.f. Figure 5(d)). Note that in Figure 6 we have explicitly plotted the unstable part of the magnetic response curves (dashed lines). In reality, micron sized magnetic cylinders will undergo an irreversible orientational transition when the magnetic field is reduced below the left most spinodal point or increased above the right most spinodal point (see Figure 5(d)).

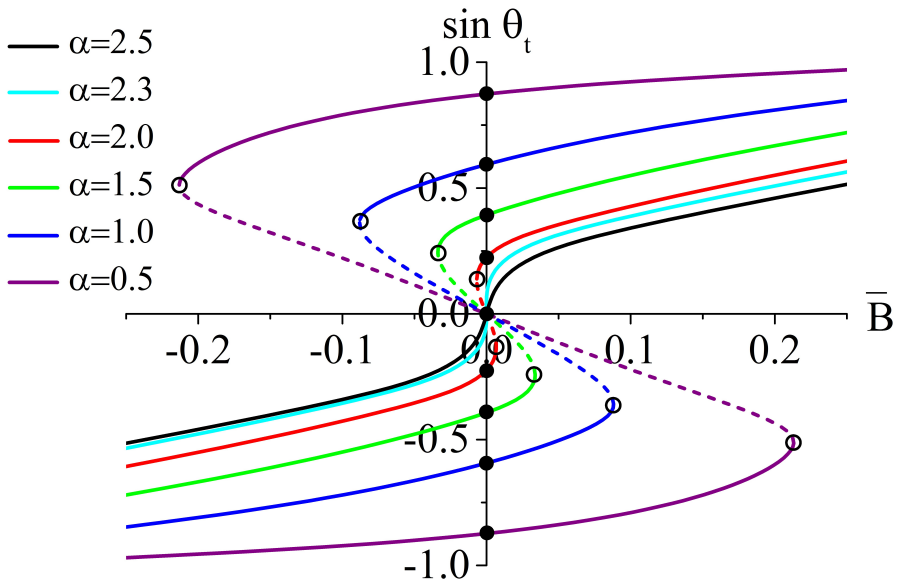

Figure 6: Surface Evolver results for the stationary tilt angles (i.e., tilt angles corresponding to minima or maxima of the free energy curves) as a function of the external field $\overline{B}$ in the low field regime for different values of α for neutrally wetting cylinders with $\eta = 20$. The solid (dashed) lines corresponding to locally stable (unstable) tilt angles. The filled and unfilled circles correspond to the binodal and spinodal points respectively when $\alpha < \alpha_c$. Note that the solid curves between the binodal and spinodal points are metastable while the rest of the solid curves are stable. See main text for details.

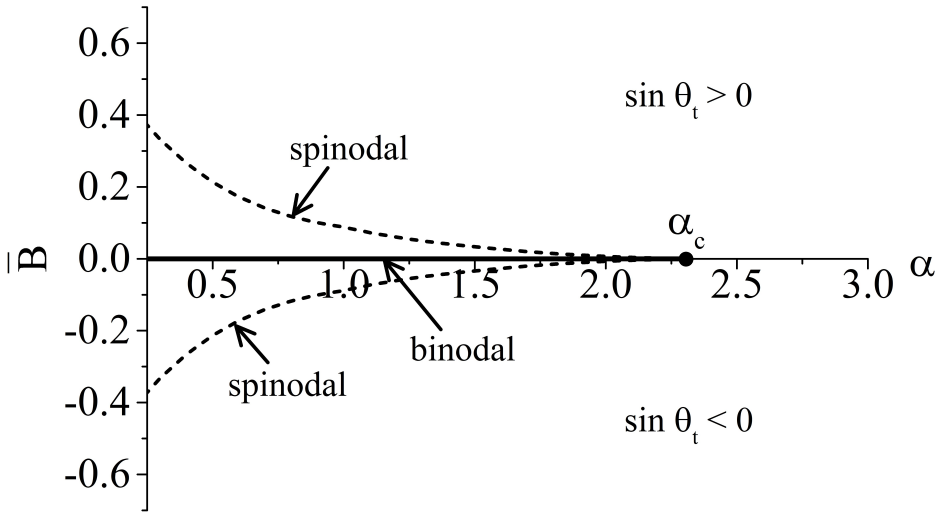

Figure 7: Phase diagram for orientational transitions of neutrally wetting magnetic cylinders in the $\overline{B}-\alpha$ plane calculated from Surface Evolver, including the binodal line (solid line), the spinodal line (dashed line) and the critical point. The thermodynamically stable tilt angle above (below) the $\overline{B}=0$ line is positive (negative).

In Figure 7 we plot the phase diagram for orientational transitions of neutrally wetting magnetic cylinders in the $\overline{B}-\alpha$ plane, including the binodal line (solid line), the spinodal line (dashed line) and the critical point $(0,\alpha_c)$. Referring to the phase diagram, for $\overline{B}>0$ and $\overline{B}<0$, the thermodynamically stable tilt angle is positive and negative respectively. For magnetic cylinders with $\alpha>\alpha_c$, as we increase the magnetic field from negative to positive, the tilt angle changes continuously from negative to positive. In contrast, for magnetic cylinders with $\alpha<\alpha_c$, as we increase the magnetic field from negative to positive, *thermodynamically*, the tilt angle changes discontinuously from negative to positive at the binodal line. However, for micron sized magnetic cylinders, *kinetically*, the tilt angle will change discontinuously from negative to positive only at the upper spinodal line. For all values of α, analogous behaviour also occurs as we decrease the magnetic field from positive to negative. Finally, we can find the locally stable tilt angle in all the cases discussed above by using the magnetic response curve for the relevant α value given in Figure 6.

In order to analyse the response of the meniscus deformation to particle tilt, in Figure 8 we plot Surface Evolver results for the difference in the maximal and minimal height

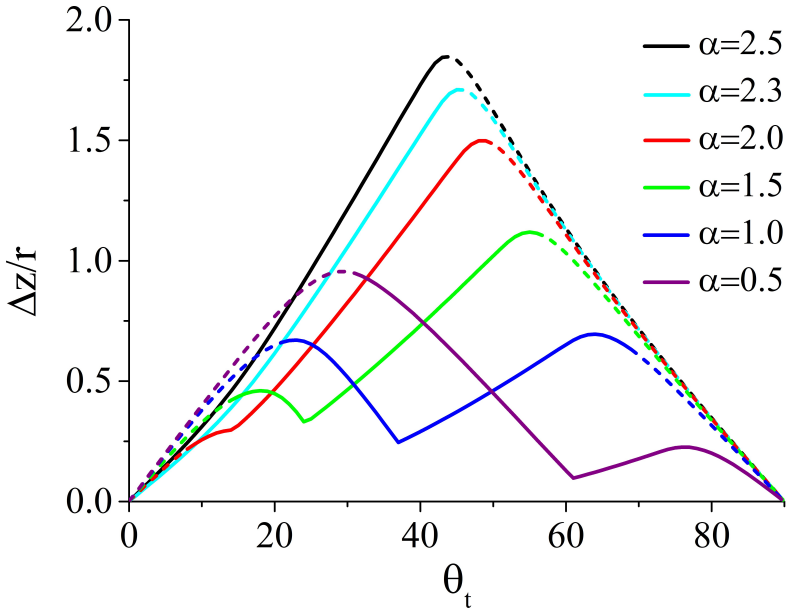

Figure 8: The difference in the maximal and minimal height along the contact line (normalised with respect to r) $\Delta z/r$ as a function of tilt angle for neutrally wetting cylinders for different values of α. Tilt angles which are accessible (inaccessible) through varying the external field are plotted as solid (dashed) lines. See main text for details.

along the contact line at the particle (normalised with respect to r), i.e., $\Delta z/r$, as a function of tilt angle for cylinders with $\theta_w = 90°$ and different values of α. Only positive values of θ_t are considered in Figure 8 since the plots are symmetric about $\theta_t = 0°$. We note that $\Delta z/r$ can be measured experimentally using phase shift interferometry (PSI).[17,35] Referring to Figure 5(b) and (d), only some tilt angles θ_t are accessible through varying the external field, specifically $|\theta_t| \leq |\theta_{c2}|$ for $\alpha > \alpha_c$ and $|\theta_{c1}| \leq |\theta_t| \leq |\theta_{c3}|$ for $\alpha < \alpha_c$ and the accessible (inaccessible) tilt angles are plotted as solid (dashed) lines in Figure 8. We see that for $\alpha > \alpha_c$, the $\Delta z/r$ curves do not exhibit any minima (except for the trivial one at $\theta_t = 0°$), while for $\alpha < \alpha_c$, the curves exhibit a minima at the equilibrium tilt angle for that α. The minima in $\Delta z/r$ thus serve as a signature for equilibrium tilted states which can be readily verified experimentally.

To further analyse the response of the meniscus deformation on particle tilt, in Figure 9 we plot Surface Evolver results for the area enclosed by the undulating contact line projected onto the unperturbed interfacial plane S as a function of tilt angle for cylinders with $\theta_w = 90°$ and for the same range of α as shown in Figure 8. The projected area S for each α is normalised with respect to the projected area at zero tilt angle S_0. Once again,

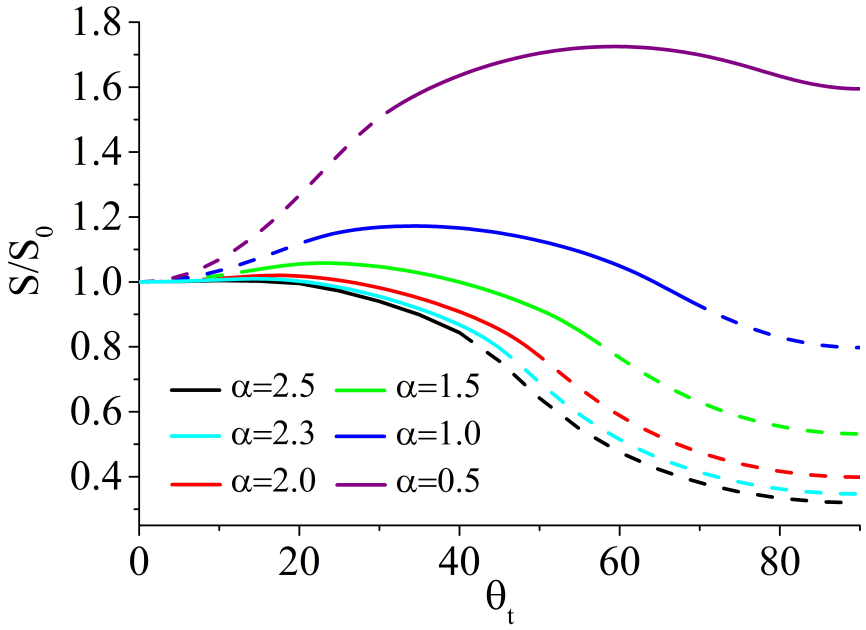

Figure 9: Surface Evolver results for the (normalised) projected area enclosed by the undulating contact line as a function of tilt angle for neutrally wetting cylinders with the same range of α as shown in Figure 8. Tilt angles which are accessible (inaccessible) through varying the external field are plotted as solid (dashed) lines. See main text for details.

only positive values of θ_t are considered in Figure 9 since the plots are symmetric about $\theta_t = 0°$ and accessible (inaccessible) tilt angles are plotted as solid (dashed) lines. Note that the quantity S/S_0 can also be measured experimentally using PSI under reflection illumination.[17,35] We see that for $\alpha > \alpha_c$, the S/S_0 curves do not exhibit any maxima (except for the trivial one at $\theta_t = 0°$), while for $\alpha < \alpha_c$, each curve exhibits a broad maxima at the equilibrium tilt angle for that α. The maxima in S/S_0 thus serve as an additional signature for tilted states which can be readily verified experimentally.

3.2 Non-neutrally Wetting Cylinders ($\theta_w \neq 90°$)

We next study the orientation and magnetic response of non-neutrally wetting particles. Lewandowski et al.[10] showed that for a given aspect ratio α, changing the contact angle θ_w away from 90° stabilises the end-on state relative to the side-on state. This is because when $\theta_w \neq 90°$, the contact line in the end-on state is positioned at the corner of the cylinder so that, as we change θ_w away from 90°, the area of liquid interface removed by the cylinder is essentially unchanged for the end-on state, but it is decreased for the side-on state. This means that we can use θ_w, in addition to α, to engineer the orientational

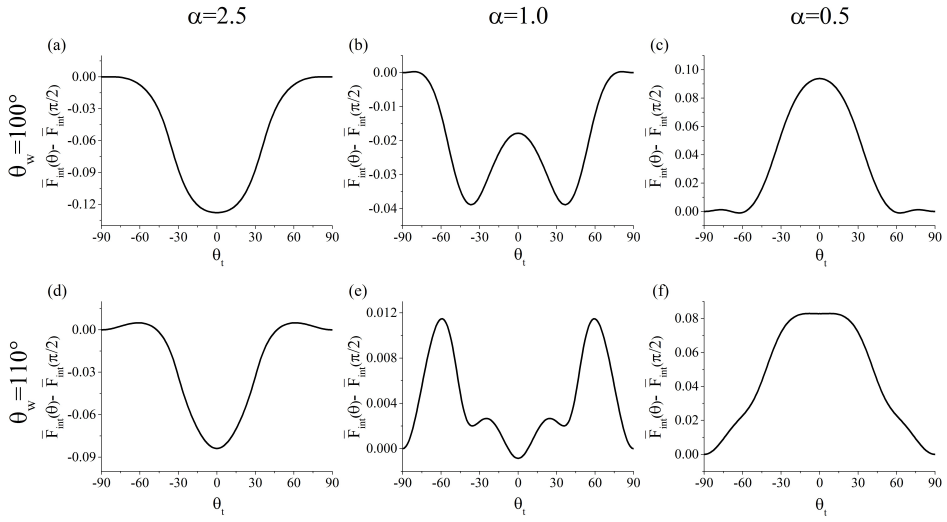

Figure 10: Surface Evolver results for the dimensionless free energy (relative to the end-on state) as a function of tilt angle for cylinders in the absence of an external field with $\eta = 20$ and different aspect ratios α and contact angles θ_w.

free energy landscape, and hence the magnetic response, of cylindrical particles.

In Figure 10 we plot Surface Evolver results for the dimensionless free energy as a function of tilt angle for contact angles $\theta_w = 100°, 110°$ and aspect ratios $\alpha = 2.5, 1.0, 0.5$ in the absence of an external field. In Figure 2 in Supplementary Information, the free energy curves are plotted over the same range of α and θ_w but for more intermediate values in order to obtain a higher resolution picture of how changing θ_w and α impacts the orientational free energy landscape. From these results, we see that for a given $\theta_w \neq 90°$, as we reduce α below a critical value α_c, the free energy curve at small tilt angles undergoes spontaneous symmetry breaking into two equivalent tilted states as before. However, these results also suggest that increasing the contact angle away from $\theta_w = 90°$ leads to a decrease in α_c.

In order to determine the value of α_c at each contact angle θ_w, we performed Surface Evolver simulations at small θ_t with a resolution of 0.1 in α. The critical aspect ratio was then determined from the value of α where the curvature at $\theta_t = 0$ changed sign. The results for α_c as a function of θ_w are tabulated in the Supplementary Information. Note that we only need to perform simulations for $\theta_w > 90°$ since the α_c values are symmetric about $\theta_w = 90°$. These results confirm that α_c indeed decreases as we change the contact angle away from $\theta_w = 90°$. Note that for $\theta_w > 105°$ and small values of α, the shape of the free energy curve at small tilt angles θ_t becomes increasingly complex such that a simple curvature analysis of the free energy curves at $\theta_t = 0°$ from which α_c is derived

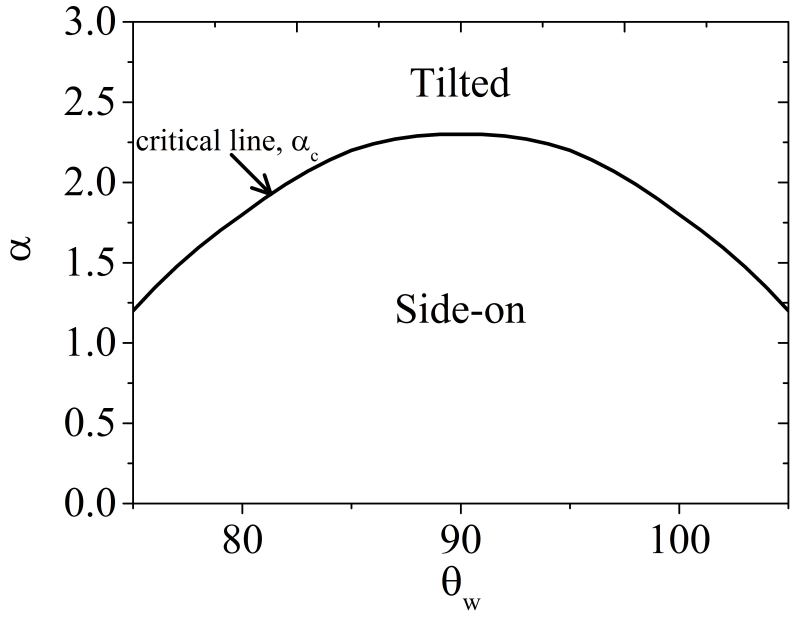

Figure 11: Phase diagram for magnetic cylinders in the $\alpha - \theta_w$ plane for zero external field calculated from Surface Evolver, including the critical line for the side-on to tilted state transition.

is no longer very meaningful (see last row of Figure 2 in Supplementary Information). We have therefore only calculated α_c for contact angles in the range $\theta_w = 75° \rightarrow 105°$. In Figure 11, we plot the phase diagram for magnetic cylinders in the $\alpha - \theta_w$ plane for zero external field, including the critical line for the side-on to tilted state transition. Note that the phase diagram in Figure 11 looks very different from the one given in ref.[10] because the authors in ref.[10] only considered cylinders in the end-on or side on states while we have included the possibility of the cylinders being in intermediate tilted states.

Next, from Figures 3 and 10 and Figure 2 in Supplementary Information, we see that for a given α, increasing θ_w stabilises the end-on state relative to the side-on state, in good agreement with the predictions of Lewandowski et al.[10] However, by analysing all particle orientations and not just the end-on and side-on states, our calculations show that increasing θ_w also causes the end-on state to become *locally* stable, e.g., compare Figure 10(a) to Figure 10(d) and Figure 3(b) to Figure 10(b). Indeed for $\alpha = 0.5$, increasing the contact angle from $\theta_w = 100°$ to $\theta_w = 110°$ causes the end-on state to become the globally stable state (Figure 10(f)). Thus, by tuning *both* θ_w and α, we can design cylindrical systems with more than two stable orientations and hence create switchable materials with unique magnetic responses that have no analogs in simple

paramagnetic or ferromagnetic systems.

We first consider the case $\alpha = 2.5$ and $\theta_w = 110^\circ$ (Figure 10(d)). Since $\alpha > \alpha_c$, the side-on state is stable while the fact that $\theta_w = 110^\circ$ means that the two end-on states are also (locally) stable. We therefore have a system with *three* stable orientations in the absence of an external field. The response of this system to an external field is shown in Figure 12(a). For definiteness, let us assume that the magnetic cylinder is initially in the negative end-on state ($\theta_t = -90^\circ$) in zero field, i.e., bottom filled circle in Figure 12(a). As we increase the external field, the cylinder remains in the negative end-on state until the field is equal to the critical value $\overline{B}_{c1}$, when the cylinder undergoes an irreversible transition to a positive tilted state. At this point, if we decrease the field to zero, we can access the side-on state of the cylinder, i.e., the middle filled circle in Figure 12(a). On the other hand, if we increase the field from $\overline{B}_{c1}$, the equilibrium tilt angle will increase until the field is equal to the critical value $\overline{B}_{c2}$, when the particle undergoes an irreversible transition to the positive end-on state ($\theta_t = 90^\circ$). At this point, if we decrease the field to zero, the positive end-on state remains stable, i.e., top filled circle in Figure 12(a). Analogous behaviour to everything discussed above will also occur for $\overline{B} < 0$ (see Figure 12(a)).

We next consider the case $\alpha = 1.0$ and $\theta_w = 100^\circ$ (Figure 10(b)). Since $\alpha < \alpha_c$, two equivalent tilted states are stable while the fact that $\theta_w = 100^\circ$ means that the two end-on states are also stable. Note that although the dimensionless energy barrier stabilising the end-on states are small ($\Delta\overline{F}_{int} \approx 2.5 \times 10^{-4}$), for micron sized particles (say $r = 1\mu$m) at an oil/water interface (say $\gamma = 30$mN/m), this barrier corresponds to a value of $4 \times 10^4 k_B T$ so that the end-on state is thermally stable. We therefore have a system with *four* stable orientations in the absence of an external field. The response of this system to an external field is shown in Figure 12(b). For definiteness, let us assume that the magnetic cylinder is initially in the negative end-on state ($\theta_t = -90^\circ$) in zero field, i.e., bottom filled circle in Figure 12(b). As we increase the external field, the cylinder remains in the negative end-on state until the field is equal to the critical value $\overline{B}_{c1}$, when the cylinder undergoes an irreversible transition to a negative tilted state. At this point, if we decrease the field to zero, we can access the negative tilted state of the cylinder corresponding to the second filled circle from the bottom in Figure 12(b). On the other hand, if we increase the field from $\overline{B}_{c1}$, the equilibrium tilt angle will increase until

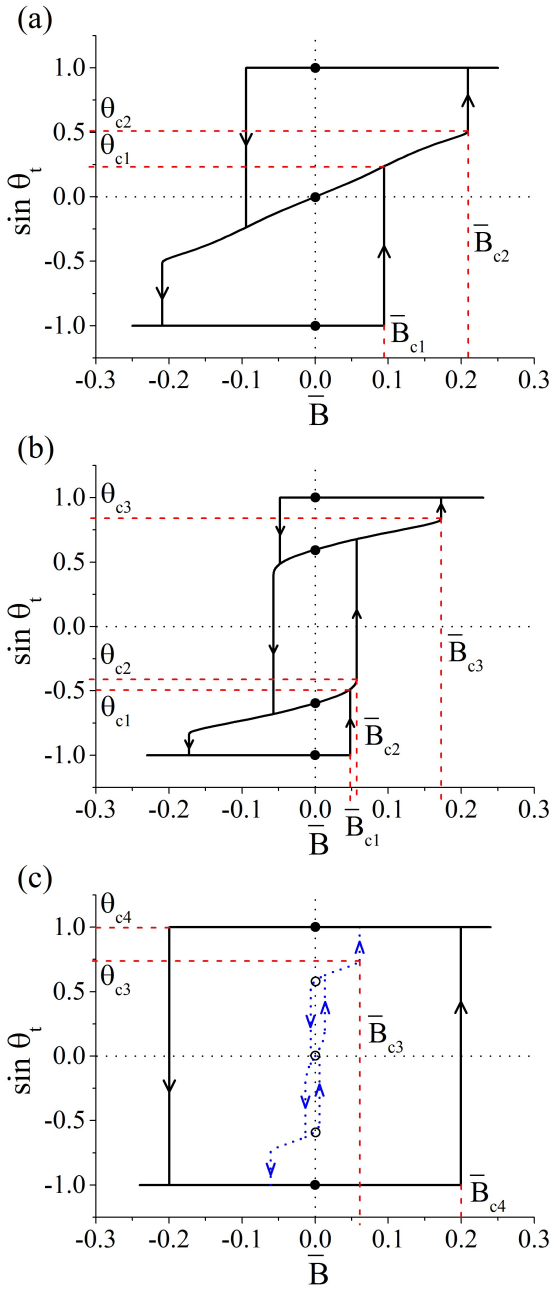

Figure 12: Surface Evolver results for the locally stable tilt angle as a function of field strength for cylinders with $\eta = 20$ and different combinations of α and θ_w. (a) $\alpha = 2.5$, $\theta_w = 110°$; (b) $\alpha = 1.0$, $\theta_w = 100°$; (c) $\alpha = 1.0$, $\theta_w = 110°$. The vertical lines represent irreversible orientational transitions, with the direction of the transition as indicated by the arrows. For all the other solid lines, it is possible to change the tilt angle along the line in either direction by changing the external field. The filled circles represent locally stable particle orientations at zero field. In (c), the dashed lines and open circles represent parts of the magnetic response that are not accessible once the external field exceeds $\overline{B}_{c3}$. See main text for details.

the field is equal to the critical value $\overline{B}_{c2}$, when the particle undergoes an irreversible transition to a positive tilted state. At this point, if we decrease the field to zero, we can access the positive tilted state of the cylinder corresponding to the third filled circle from the bottom in Figure 12(b). On the other hand, if we increase the field from $\overline{B}_{c2}$, the equilibrium tilt angle will increase until the field is equal to the critical value $\overline{B}_{c3}$, when the particle undergoes an irreversible transition to a positive tilted state. At this point, if we decrease the field to zero, the positive end-on state remains stable, i.e., top filled circle in Figure 12(b). Once again, analogous behaviour to everything discussed above will also occur for $\overline{B} < 0$ (see Figure 12(b)).

Finally, we consider the case $\alpha = 1.0$ and $\theta_w = 110^\circ$ (Figure 10(e)). The orientational energy landscape in this case is very complex, with *five* stable orientations in the absence of an external field, including the side-on state, two tilted states and two end-on states. However, from the magnetic response of this system in Figure 12(c), we see that, regardless of the initial state of the cylinder, once the magnetic field exceeds the critical value $\overline{B}_{c3}$, only the two end-on states (i.e., filled circles in Figure 12(c)) are accessible while the other three states (i.e., open circles in Figure 12(c)) are no longer accessible. In summary, from the point of view of creating non-volatile switchable materials, the key feature of Figure 12 is the fact that it is possible to use both α and θ_w to engineer cylinders that have three or even four locally stable orientations which can be accessed by varying the external field.

We now assess the feasibility of inducing the above orientational transitions experimentally. For definiteness, we will focus on the three stable state system shown in Figure 12(a). For a typical micron-sized system possessing a permanent magnetic dipole, we use parameters for anisotropic maghemite (γ-Fe_2O_3) particles.[36,37] Assuming cylinders with radius $r = 1\mu$m and aspect ratio $\alpha = 2.5$, this yields a magnetic dipole moment $m = 5 \times 10^{-12}\text{A}\cdot\text{m}^{-2}$. The dimensionless critical field for the tilt to perpendicular transition is $\overline{B}_{c2} \approx 0.2$. Using a typical oil/water tension of $\gamma_{ow} = 30\text{mN/m}$, this translates to a magnetic field of $B = 0.05\text{T}$, which is readily achievable experimentally. Interestingly, the estimated magnetic field required to induce reorientation of cylindrical particles is of the same order as those predicted in ref.[16] for ellipsoidal particles made from the same material with a similar size and aspect ratio. This fact points to the generality of the predicted orientational transitions and the feasibility of observing such transitions in a

variety of particle shapes.

Finally, although the primary focus of this paper has been to use an external field to control the *orientation* of individual cylindrical particles at a liquid interface, since orientation is coupled to meniscus deformation and hence capillary interactions between particles, we can also use an external field to control the *self-assembly* of multiple particle systems. Switchable self-assembly has already been demonstrated in the work of Davies et al. for magnetic ellipsoids[5] and we can exploit the same effect to control the self-assembly of magnetic cylinders. For example, for the three state system shown in Figure 12(a), the particles interact with each other via quadrupolar capillary interactions when they are in the side-on state[11] but they do not interact with each other in the end-on state because the meniscus is flat in this case. Similarly, for the four state system shown in Figure 12(b), the particles interact with each other via hexapolar capillary interactions when they are in the tilted state (Figure 4)[33] but they do not interact with each other in the end-on state. The key advantage of using cylinders instead of ellipsoids in this context is that the switching of the self-assembly for cylinders is again *non-volatile*. For future work, we will study both orientation and capillary deformations in multiple particle systems.

4 Conclusion

We have studied the influence of an external magnetic field on the orientation of single magnetic cylinders at a liquid interface using a simple flat interface model as well as high resolution Surface Evolver simulations which take into account the deformation of the liquid meniscus around the particle. We have shown that, in the absence of an external field, as we reduce the aspect ratio α of the cylinders below a critical value, the particles undergo spontaneous symmetry breaking from a stable side-on state to one of two equivalent stable tilted states, similar to the spontaneous magnetisation of a ferromagnet going through the Curie point. Similar tilted states have been predicted for anisotropic Janus particles,[3,28–30] but to our knowledge this is the first time that their existence has been discussed explicitly for anisotropic colloids with homogeneous surface chemistry. Furthermore, by tuning both the aspect ratio and contact angle of the cylinder, we have shown that it is possible to engineer particles that have one, two, three or four locally stable orientations and that it is possible to induce non-volatile transitions between these

states by varying the external field. We found that that the magnetic response of systems with one or two stable states is similar to that of paramagnets and ferromagnets respectively, while the magnetic response of systems with three or four stable states have no analogs in simple magnetic systems. We have also shown that for micron sized cylinders with realistic magnetic moments, the critical fields required to access the different stable orientations are accessible experimentally. Finally, although this paper focusses on using external fields to control the orientation of individual magnetic cylinders, since particle orientation at a liquid interface is coupled to capillary interactions between particles, it is also possible to use an external field to control the *self-assembly* of multiple cylinders. Magnetic cylinders at liquid interfaces therefore provide an exciting new approach for creating switchable functional surfaces where we can use an external field to induce multiple *non-volatile* changes in optical, magnetic and mechanical properties. Note that the detailed structure of the self-assembled aggregates is governed by near-field capillary interactions[18,19,21] and many body forces[38] but our understanding of how these forces control the self-assembly of anisotropic particles is still at an early stage. For future work, we will study both orientation and capillary deformations in systems consisting of multiple anisotropic particles.

Acknowledgments

BJN is grateful to The University of Hull, The Joseph and Annie Cattle Trust, The Elizabeth Walker Foundation and The Ann Watson's Trust for financial support. We thank Professor Kenneth Brakke for his guidance on using Surface Evolver. We also thank one of the referees for their insightful comments which have greatly improved the paper.

References

1. Binks, B. P.; Horozov, T. S., Eds.; *Colloidal Particles at Liquid Interfaces;* Cambridge University Press: Cambridge, 2006.

2. Günther, F.; Frijters, S.; Harting, J. *Soft Matter* **2014,** *10,* 4977.

3. Bromley, K. M.; Morris, R. J.; Hobley, L.; Brandani, G.; Gillespie, R. M. A.; McCluskey, M.; Zachariae, U.; Marenduzzo, D.; Stanley-Wall, N. R.; MacPhee, C. E. *Proc. Natl. Acad. Sci. U.S.A.* **2015,** *112,* 5419.

4. Law, A. D.; Auriol, M.; Smith, D.; Horozov, T. S.; Buzza, D. M. A. *Phys. Rev. Lett.* **2013,** *110,* 138301.

5. Davies, G. B.; Krüger, T.; Coveney, P. V.; Harting, J.; Bresme, F. *Advanced Materials* **2014,** *26,* 6715.

6. Loudet, J. C.; Alsayed, A. M.; Zhang, J.; Yodh, A. G. *Phys. Rev. Lett.* **2005,** *94,* 018301.

7. Loudet, J. C.; Yodh, A. G.; Pouligny, B. *Phys. Rev. Lett.* **2006,** *97,* 018304.

8. Lehle, H.; Noruzifar, E.; Oettel, M. *Eur. Phys. J. E* **2008,** *26,* 151.

9. Oettel, M.; Dietrich, S. *Langmuir* **2008,** *24,* 1425.

10. Lewandowski, E. P.; Searson, P. C.; Stebe, K. J. *Journal of Physical Chemistry B* **2006,** *110,* 4283.

11. Lewandowski, E. P.; Cavallaro Jr., M.; Botto, L.; Bernate, J. C.; Garbin, V.; Stebe, K. J. *Langmuir* **2010,** *26,* 15142.

12. Morris, G.; Neethling, S. J.; Cilliers, J. J. *Journal of Colloid and Interface Science* **2011,** *354,* 380.

13. Morgan, A. R.; Ballard, N.; Rochford, L. A.; Nurumbetov, G.; Skelhon, T. F.; Bon, S. A. F. *Soft Matter* **2013,** *9,* 487.

14. Bresme, F.; Faraudo, J. *J. Phys. Condens. Matter* **2007,** *19,* 375110.

15. Davies, G. B.; Krüger, T.; Coveney, P. V.; Harting, J.; Bresme, F. *Soft Matter* **2014,** *10,* 6742.

16. Newton, B. J.; Brakke, K. A.; Buzza, D. M. A. *Phys. Chem. Chem. Phys.* **2014,** *16,* 26051.

17. Dasgupta, S.; Katava, M.; Faraj, M.; Auth, T.; Gompper, G. *Langmuir* **2014,** *30,* 11873.

18. Botto, L.; Yao, L.; Leheny, R. L.; Stebe, K. J. *Soft Matter* **2012,** *8,* 4971.

19. Botto, L.; Lewandowski, E. P.; Cavallaro, M., J.; Stebe, K. J. *Soft Matter* **2012,** *8,* 9957.

20. Cooray, H.; Cicuta, P.; Vella, D. *J. Phys. Condens. Matter* **2012,** *24,* 284104.

21. Loudet, J. C.; Pouligny, B. *Europhysics Letters* **2009,** *85,* 28003.

22. Mittal, M.; Furst, E. M. *Adv. Funct. Mater.* **2009,** *19,* 3271.

23. Lumay, G.; Obara, N.; Weyer, F.; Vandewalle, N. *Soft Matter* **2013,** *9,* 1.

24. Davies, G. B.; Botto, L. *Soft Matter* **2015,** *11,* 7976.

25. Cavallaro, M. J.; Botto, L.; Lewandowski, E. P.; Wang, M.; Stebe, K. J. *Proc. Natl. Acad. Sci. U.S.A.* **2011,** *108,* 20923.

26. Ershov, D.; Sparkel, J.; Appel, J.; Cohen Stuart, M. A.; van der Gucht, J. *Proc. Natl. Acad. Sci. U.S.A.* **2013,** *110,* 9220.

27. Brakke, K. A. *Experimental Mathematics* **1992,** *1,* 141.

28. Park, B. J.; Lee, D. *ACS Nano* **2012,** *6,* 782.

29. Park, B. J.; Choi, C.-H.; Kang, S.-M.; Tettey, K. E.; Lee, C.-S.; Lee, D. *Soft Matter* **2013,** *9,* 3383.

30. Park, B. J.; Choi, C.-H.; Kang, S.-M.; Tettey, K. E.; Lee, C.-S.; Lee, D. *Langmuir* **2013,** *29,* 1841.

31. Huang, K. *Statistical Mechanics;* John Wiley & Sons: New York, 2nd ed.; 1987.

32. Stamou, D.; Duschl, C.; Johannsman, D. *Phys. Rev. E* **2000,** *62,* 5263.

33. Danov, K. D.; Kralchevsky, P. A.; Naydenov, B. N.; Brenn, G. *Journal of Colloid and Interface Science* **2005,** *287,* 121.

34. Bleaney, B. I.; Bleaney, B. *Electricity and Magnetism vol.1;* Oxford University Press: Oxford, 3rd ed.; 1976.

35. Loudet, J. C.; Pouligny, B. *Eur. Phys. J. E* **2011,** *34,* 1.

36. Mendoza-Zelis, P.; Muraca, D.; Gonzalez, J. S.; Pasquevich, G. A.; Alvarez, V. A.; Pirota, K. R.; Sanchez, F. H. *Journal of Nanoparticle Research* **2013,** *15,* 1613.

37. Hijnen, N. PhD thesis, University of Edinburgh, 2013.

38. Fournier, J. B.; Galatola, P. *Phys. Rev. E* **2002,** *65,* 031601.

Magnetic cylindrical particles at liquid interfaces exhibit non-volatile switching of their orientation in an external field.